

## – Online Appendix –

# How does joint evolution of consumer traits affect resource specialization?

Paula Vasconcelos<sup>1</sup> and Claus Rueffler<sup>1,\*</sup>

*The American Naturalist* 2019

1. Department of Ecology and Genetics, Animal Ecology, Uppsala University, Norbyvägen 18D, 752 36 Uppsala, Sweden

\* Corresponding author; e-mail: claus.rueffler@ebc.uu.se.

## A Appendix: Ecological dynamics

The unique interior equilibrium of Eq. (1) in the main part is given by

$$\hat{R}_1 = \frac{K_1(de_1r_2 - K_2X_2(r_2e_1e_2 - r_1e_2^2))}{r_2e_1^2K_1X_1 + r_1e_2^2K_2X_2} \quad (\text{A1a})$$

$$\hat{R}_2 = \frac{K_2(de_2r_1 - K_1X_1(r_1e_1e_2 - r_2e_1^2))}{r_2e_1^2K_1X_1 + r_1e_2^2K_2X_2} \quad (\text{A1b})$$

$$\hat{C} = \frac{r_1r_2(e_1K_1X_1 + e_2K_2X_2 - d)(K_1K_2e_1e_2(r_1e_2 - r_2e_1)(h_1\alpha_2 - h_2\alpha_1) + r_1K_2\alpha_2e_2^2 + r_2K_1\alpha_1e_1^2)}{(r_2e_1^2K_1X_1 + r_1e_2^2K_2X_2)^2}, \quad (\text{A1c})$$

where

$$X_1 = \alpha_1 - dh_1 \quad \text{and} \quad X_2 = \alpha_2 - dh_2.$$

Under full symmetry, that is  $e_1 = e = e_2$ ,  $h_1 = h = h_2$ ,  $\alpha_1 = \alpha = \alpha_2$ ,  $K_1 = K = K_2$ ,  $r_1 = r = r_2$ , these expressions simplify to

$$\hat{R}_1 = \frac{d}{2e(\alpha - dh)} \quad (\text{A2a})$$

$$\hat{R}_2 = \frac{d}{2e(\alpha - dh)} \quad (\text{A2b})$$

$$\hat{C} = \frac{r\alpha(2eK(\alpha - dh) - d)}{2e^2K(\alpha - dh)^2}. \quad (\text{A2c})$$

The consumer population size at equilibrium is positive if

$$2eK(\alpha - dh) > d, \quad (\text{A3})$$

## 2 *The American Naturalist*

---

which requires  $\alpha - hd > 0$ . The equilibrium point given by Eq. (A2) is an asymptotically stable fixed point if

$$2ehK < \frac{\alpha + dh}{\alpha - dh} \quad (\text{A4})$$

(e.g. Iannelli and Pugliese, 2014, p. 165). We restrict our investigation to parameters that fulfill conditions (A3) and (A4).

By adding a mutant consumer the extended dynamical system becomes

$$\frac{dR_1}{dt} = r_1 R_1 \left(1 - \frac{R_1}{K_1}\right) - \frac{R_1 e_1^r C^r}{1 + R_1 e_1^r h_1^r + R_2 e_2^r h_2^r} - \frac{R_1 e_1^m C^m}{1 + R_1 e_1^m h_1^m + R_2 e_2^m h_2^m} \quad (\text{A5a})$$

$$\frac{dR_2}{dt} = r_2 R_2 \left(1 - \frac{R_2}{K_2}\right) - \frac{R_2 e_2^r C^r}{1 + R_1 e_1^r h_1^r + R_2 e_2^r h_2^r} - \frac{R_2 e_2^m C^m}{1 + R_1 e_1^m h_1^m + R_2 e_2^m h_2^m} \quad (\text{A5b})$$

$$\frac{dC^r}{dt} = C^r \left( \frac{\alpha_1^r R_1 e_1^r + \alpha_2^r R_2 e_2^r}{1 + R_1 e_1^r h_1^r + R_2 e_2^r h_2^r} - d \right) \quad (\text{A5c})$$

$$\frac{dC^m}{dt} = C^m \left( \frac{\alpha_1^m R_1 e_1^m + \alpha_2^m R_2 e_2^m}{1 + R_1 e_1^m h_1^m + R_2 e_2^m h_2^m} - d \right), \quad (\text{A5d})$$

where the superscript r denotes resident and superscript m denotes mutant. From a linear stability analysis of this system at the equilibrium in which the mutant is absent follows that invasion fitness  $w(\theta^m, \theta^r)$  of a rare mutant consumer  $C^m$  with strategy  $\theta^m$  in a resident population with strategy  $\theta^r$  is given by Eq. (4) in the main part (Metz et al., 1992; Metz, 2008).

## B Appendix: Evolutionary dynamics of separately evolving traits

For our analytical derivations we assume full symmetry, that is, every trait that is not evolving as well as the remaining parameters are symmetric ( $r_1 = r = r_2$  and  $K_1 = K = K_2$ ). We drop these symmetry assumptions in Fig. E4.

### B.1 Feeding efficiency $e$

Given  $r_1 = r = r_2$ ,  $K_1 = K = K_2$ ,  $h_1 = h = h_2$  and  $\alpha_1 = \alpha = \alpha_2$  Eq. (A1) simplifies to

$$\hat{R}_1(\theta_e^r) = \frac{de_1(\theta_e^r) - K(\alpha - dh)(e_1(\theta_e^r)e_2(\theta_e^r) - e_2(\theta_e^r)^2)}{(\alpha - dh)(e_1(\theta_e^r)^2 + e_2(\theta_e^r)^2)} \quad (\text{B1a})$$

$$\hat{R}_2(\theta_e^r) = \frac{de_2(\theta_e^r) - K(\alpha - dh)(e_1(\theta_e^r)e_2(\theta_e^r) - e_1(\theta_e^r)^2)}{(\alpha - dh)(e_1(\theta_e^r)^2 + e_2(\theta_e^r)^2)} \quad (\text{B1b})$$

$$\hat{C}(\theta_e^r) = \frac{r\alpha(K(\alpha - dh)(e_1(\theta_e^r) + e_2(\theta_e^r)) - d)}{K(\alpha - dh)^2(e_1(\theta_e^r)^2 + e_2(\theta_e^r)^2)}. \quad (\text{B1c})$$

The selection gradient is defined as the derivative of invasion fitness  $w(\theta_e^m, \theta_e^r)$  with respect

to the mutant strategy  $\theta_e^m$  and evaluated at the resident strategy  $\theta_e^r$ ,

$$\frac{\partial w(\theta_e^m, \theta_e^r)}{\partial \theta_e^m} \Big|_{\theta_e^m=\theta_e^r} = \frac{\alpha(\hat{R}_1(\theta_e^r)e'_1(\theta_e^r) + \hat{R}_2(\theta_e^r)e'_2(\theta_e^r))}{(1 + he_1(\theta_e^r)\hat{R}_1(\theta_e^r) + he_2(\theta_e^r)\hat{R}_2(\theta_e^r))^2}. \quad (\text{B2})$$

A trait value at which the selection gradient vanishes is termed a singular point. Due to the symmetry of the trade-off parametrization given by Eq. (2) in the main part at the generalist's trait value  $\theta_e^r = 0.5$  we have  $e_1(0.5) = e_2(0.5)$  and  $e'_1(0.5) = -e'_2(0.5)$ . Thus, Eq. (B2) evaluates to zero for  $\theta_e^r = 0.5$ , since this makes  $\hat{R}_1(\theta_e^r) = \hat{R}_2(\theta_e^r)$  and  $e'_1(\theta_e^r) = -e'_2(\theta_e^r)$ . Thus,  $\theta_e^* = 0.5$  is a singular point. Numerical evaluation of Eq. (B2) set equal to zero reveals the existence of two flanking singular points for moderately weak trade-off as shown in Fig. 4a in the main part.

We note that at the symmetric singular point  $\theta_e^* = 0.5$  we have

$$e(\theta_e^*) := e_1(\theta_e^*) = e_2(\theta_e^*) \quad e'(\theta_e^*) := e'_1(\theta_e^*) = -e'_2(\theta_e^*) < 0 \quad e''(\theta_e^*) := e''_1(\theta_e^*) = e''_2(\theta_e^*) \quad (\text{B3})$$

and

$$\hat{R}(\theta_e^*) := \hat{R}_1(\theta_e^*) = \hat{R}_2(\theta_e^*) \quad \hat{R}'(\theta_e^*) := \hat{R}'_1(\theta_e^*) = -\hat{R}'_2(\theta_e^*) > 0. \quad (\text{B4})$$

For later use we note that

$$\hat{R}'(\theta_e^*) = \frac{e' (d - 2eK(\alpha - dh))}{2e^2(\alpha - dh)}, \quad (\text{B5})$$

which equals zero if and only if equality holds for (A3), i.e., if the consumer density equals  $\hat{C} = 0$ .

From Eqs. (B1a) and (B1b) follows that

$$\hat{R}_1(\theta_e^r) \gtrless \hat{R}_2(\theta_e^r) \iff (e_2(\theta_e^r) - e_1(\theta_e^r))(K(\alpha - dh)(e_1(\theta_e^r) + e_2(\theta_e^r)) - d) \gtrless 0. \quad (\text{B6})$$

The second factor on the left-hand side of the right inequality is positive whenever the consumer equilibrium given by Eq. (B1c) is positive. With this we can conclude that the resource for which the resident consumer has a higher feeding efficiency is less abundant.

To determine whether a singular point is invadable by nearby mutants, we need to know whether it is a local fitness minimum or fitness maximum. In order to find out, we determine the second derivative of invasion fitness with respect to the mutant evaluated at the singular point. If the singular point is a fitness minimum, the sign of the second derivative is positive, whereas if it is a fitness maximum, the sign of the second derivative is negative. We find

$$\frac{\partial^2 w(\theta_e^m, \theta_e^r)}{\partial \theta_e^m^2} \Big|_{\theta_e^m=\theta_e^r=\theta_e^*} = \frac{2e''(\theta_e^*)\alpha\hat{R}(\theta_e^*)}{(1 + 2he(\theta_e^*)\hat{R}(\theta_e^*))^2}. \quad (\text{B7})$$

The sign of Eq. (B7) is determined by the sign of  $e''(\theta_e^*)$ . Since  $e''(\theta_e^*) < 0$  for  $z_e > 0$  and  $e''(\theta_e^*) > 0$  for  $z_e < 0$  it follows that Eq. (B7) is negative for positive values of  $z_e$  and positive

#### 4 *The American Naturalist*

---

for negative values of  $z_e$ . This means that the singular point  $\theta_e^*$  is unininvadable when the trade-off is weak and invadable when the trade-off is strong.

A singular point is an attractor of the evolutionary dynamics if the derivative of the selection gradient, evaluated at the singular point, is negative (Geritz et al., 1998). Otherwise, a singular point is an evolutionary repeller. The expression for this derivative is

$$\left( \frac{\partial^2 w(\theta_e^m, \theta_e^r)}{\partial \theta_e^m \partial \theta_e^r} + \frac{\partial^2 w(\theta_e^m, \theta_e^r)}{\partial \theta_e^r \partial \theta_e^m} \right) \Big|_{\theta_e^m = \theta_e^r = \theta_e^*} = \frac{2\alpha(\hat{R}(\theta_e^*)e''(\theta_e^*) + \hat{R}'(\theta_e^*)e'(\theta_e^*))}{(1 + 2h\hat{R}(\theta_e^*)e(\theta_e^*))^2}. \quad (\text{B8})$$

Since  $e'(\theta_e^*) < 0$  and  $\hat{R}'(\theta_e^*) > 0$  this expression is always negative for weak trade-offs ( $e''(\theta_e^*) < 0$  for  $z_e > 0$ ). This means that the singular point is always attracting when the trade-off is weak. For negative values of  $z_e$ , the sign of Eq. (B8) depends on the magnitude of  $\hat{R}(\theta_e^*)e''(\theta_e^*)$ , which is now positive, relative to  $e'(\theta_e^*)\hat{R}'(\theta_e^*)$ , which is negative. This numerator remains negative for moderately strong trade-off. But with increasingly stronger trade-offs the numerator becomes positive, turning the singular point into an evolutionary repeller. These results are visualized in Fig. 4a,c in the main part.

#### B.2 Handling time $h$

Under the symmetry assumptions  $r_1 = r = r_2$ ,  $K_1 = K = K_2$ ,  $e_1 = e = e_2$  and  $\alpha_1 = \alpha = \alpha_2$  Eqs. (A1a) and (A1b) simplify to

$$\hat{R}_i(\theta_h^r) = \frac{d}{e(2\alpha - d(h_1(\theta_h^r) + h_2(\theta_h^r)))} \quad \text{for } i \in \{1, 2\}. \quad (\text{B9})$$

The selection gradient for  $h$  evolving by itself equals

$$\frac{\partial w(\theta_h^m, \theta_h^r)}{\partial \theta_h^m} \Big|_{\theta_h^m = \theta_h^r} = -\frac{\alpha e^2 (\hat{R}_1(\theta_h^r) + R_2(\theta_h^r)) (h'_1(\theta_h^r)\hat{R}_1(\theta_h^r) + h'_2(\theta_h^r)\hat{R}_2(\theta_h^r))}{(1 + h_1(\theta_h^r)\hat{R}_1(\theta_h^r)e + h_2(\theta_h^r)\hat{R}_2(\theta_h^r)e)^2}. \quad (\text{B10})$$

Due to the symmetry of the trade-off parametrization given by Eq. (3) in the main part, the gradient can only be zero for  $\theta_h^r = 0.5$ , where  $h'_1(\theta_h^r) = -h'_2(\theta_h^r)$  and  $\hat{R}_1(\theta_h^r) = \hat{R}_2(\theta_h^r)$ . Thus,  $\theta_h^* = 0.5$  is a unique singular point.

We use that at the singular point  $\theta_h^* = 0.5$  we have

$$h(\theta_h^*) := h_1(\theta_h^*) = -h_2(\theta_h^*) \quad h'(\theta_h^*) := h'_1(\theta_h^*) = -h'_2(\theta_h^*) > 0 \quad h''(\theta_h^*) := h''_1(\theta_h^*) = h''_2(\theta_h^*). \quad (\text{B11})$$

and

$$\hat{R}(\theta_h^*) := \hat{R}_1(\theta_h^*) = \hat{R}_2(\theta_h^*) \quad \hat{R}'(\theta_h^*) := \hat{R}'_1(\theta_h^*) = \hat{R}'_2(\theta_h^*). \quad (\text{B12})$$

The condition for invadability then evaluates to

$$\frac{\partial^2 w(\theta_h^m, \theta_h^r)}{\partial \theta_h^m \partial \theta_h^r} \Big|_{\theta_h^m = \theta_h^r = \theta_h^*} = -\frac{4\alpha h''(\theta_h^*) \hat{R}(\theta_h^*)^2 e^2}{(1 + 2e\hat{R}(\theta_h^*)h(\theta_h^*))^2}. \quad (\text{B13})$$

Since the sign of Eq. (B13) is determined by the sign of  $h''(\theta_h^*)$ , which is negative when  $z_h < 0$  and positive when  $z_h > 0$ , the singular point  $\theta_h^*$  is invadable for strong trade-offs and unininvadable for weak trade-offs.

Using Eqs. (B11) and (B12) we find that

$$\frac{\partial^2 w(\theta_h^m, \theta_h^r)}{\partial \theta_h^m \partial \theta_h^r} \Big|_{\theta_h^m = \theta_h^r = \theta_h^*} = 0, \quad (\text{B14})$$

and therefore the conditions for attractivity and invadability are identical to each other. Thus, when only handling time  $h$  is evolving the singular point  $\theta_h^* = 0.5$  is an unininvadable attractor for weak trade-offs and an invadable repeller for strong trade-offs. The same conclusion can be reached by using the theory developed in Metz et al. (2008). For this particular case, one can prove that the trait value  $\theta_h^r$  that minimizes (maximizes)  $\hat{R}(\theta_h^r)$  as given by Eq. (B9) is an unininvadable attractor (invadable repeller).

### B.3 Conversion efficiency $\alpha$

Under the symmetry assumptions  $r_1 = r = r_2$ ,  $K_1 = K = K_2$ ,  $e_1 = e = e_2$  and  $h_1 = h = h_2$  Eqs. (A1a) and (A1b) simplify to

$$\hat{R}_i(\theta_\alpha^r) = \frac{d}{e(\alpha_1(\theta_\alpha^r) + \alpha_2(\theta_\alpha^r) - 2dh)} \quad \text{for } i \in \{1, 2\}. \quad (\text{B15})$$

The selection gradient for  $\alpha$  evolving by itself equals

$$\frac{\partial w(\theta_\alpha^m, \theta_\alpha^r)}{\partial \theta_\alpha^m} \Big|_{\theta_\alpha^m = \theta_\alpha^r} = \frac{e(\alpha'_1(\theta_\alpha^r)\hat{R}_1(\theta_\alpha^r) + \alpha'_2(\theta_\alpha^r)\hat{R}_2(\theta_\alpha^r))}{1 + eh(\hat{R}_1(\theta_\alpha^r) + \hat{R}_2(\theta_\alpha^r))}. \quad (\text{B16})$$

This gradient can only be zero when  $\theta_\alpha = 0.5$  where  $\alpha'_1(\theta_\alpha) = -\alpha'_2(\theta_\alpha)$  and  $\hat{R}_1(\theta_\alpha^r) = \hat{R}_2(\theta_\alpha^r)$ . Thus,  $\theta_\alpha^* = 0.5$  is a unique singular point.

We use that at the singular point  $\theta_\alpha^* = 0.5$  we have

$$\alpha(\theta_\alpha^*) := \alpha_1(\theta_\alpha^*) = -\alpha_2(\theta_\alpha^*) \quad \alpha'(\theta_\alpha^*) := \alpha'_1(\theta_\alpha^*) = -\alpha'_2(\theta_\alpha^*) < 0 \quad \alpha''(\theta_\alpha^*) := \alpha'_1(\theta_\alpha^*) = \alpha''_2(\theta_\alpha^*). \quad (\text{B17})$$

and

$$\hat{R}(\theta_\alpha^*) := \hat{R}_1(\theta_\alpha^*) = \hat{R}_2(\theta_\alpha^*) \quad \text{and} \quad \hat{R}'(\theta_\alpha^*) := \hat{R}'_1(\theta_\alpha^*) = \hat{R}'_2(\theta_\alpha^*). \quad (\text{B18})$$

## 6 *The American Naturalist*

---

The condition for invadability then evaluates to

$$\frac{\partial^2 w(\theta_\alpha^m, \theta_\alpha^r)}{\partial \theta_\alpha^m \partial \theta_\alpha^r} \Big|_{\theta_\alpha^m = \theta_\alpha^r = \theta_\alpha^*} = \frac{2\alpha''(\theta_\alpha^*) \hat{R}(\theta_\alpha^*) e}{1 + 2h\hat{R}(\theta_\alpha^*) e}. \quad (\text{B19})$$

Since the sign of Eq. (B19) is determined by the sign of  $\alpha''(\theta_\alpha^*)$ , which is positive when  $z_\alpha < 0$  and negative when  $z_\alpha > 0$ , the singular point  $\theta_\alpha^*$  is invadable for strong trade-offs and unininvadable for weak trade-offs.

Using Eqs. (B17) and (B18) we find that

$$\frac{\partial^2 w(\theta_\alpha^m, \theta_\alpha^r)}{\partial \theta_\alpha^m \partial \theta_\alpha^r} \Big|_{\theta_\alpha^m = \theta_\alpha^r = \theta_\alpha^*} = 0, \quad (\text{B20})$$

and therefore the conditions for attractivity and invadability are identical to each other. Thus, when only conversion efficiency  $\alpha$  is evolving the singular point  $\theta_\alpha^* = 0.5$  is an unininvadable attractor for weak trade-offs and an invadable repeller for strong trade-offs. For this particular case, one can prove that the trait value  $\theta_\alpha^r$  that minimizes (maximizes)  $\hat{R}(\theta_\alpha^r)$  as given by Eq. (B15) is an unininvadable attractor (invadable repeller) (Metz et al., 2008).

## C Appendix: Joint evolutionary dynamics

Here, we present results for the joint evolution of several traits. We omit some expressions, such as determinants and traces, due to their length and the fact that we cannot gain insight from them without evaluating them numerically. Also, since results for the joint evolution of feeding and conversion efficiency are analogous to those of the joint evolution of feeding efficiency and handling time, we do not present them here. The complete derivation and numerical analysis is available in a Mathematica notebook (Wolfram Research, Inc., 2019) deposited in the Dryad Digital Repository: <https://doi.org/10.5061/dryad.ns1rn8pnf> (Vasconcelos and Rueffler, 2019).

### C.1 Joint evolution of feeding efficiency and handling time

Under the symmetry assumptions  $r_1 = r = r_2$ ,  $K_1 = K = K_2$ , and  $\alpha_1 = \alpha = \alpha_2$  the selection gradient for the joint evolution of  $e$  and  $h$  evaluated at the vector  $\theta_{e,h}^m = \theta_{e,h}^r$  has the entries

$$S_e(\theta_{e,h}^r) = \frac{\alpha(\hat{R}_1 e'_1(\theta_e^r) + \hat{R}_2 e'_2(\theta_e^r) + \hat{R}_1 \hat{R}_2 (h_1(\theta_h^r) - h_2(\theta_h^r)) (e_1(\theta_e^r) e'_2(\theta_e^r) - e'_1(\theta_e^r) e_2(\theta_e^r)))}{(1 + h_1(\theta_h^r) \hat{R}_1 e_1(\theta_e^r) + h_2(\theta_h^r) \hat{R}_2 e_2(\theta_e^r))^2} \quad (\text{C1a})$$

$$S_h(\theta_{e,h}^r) = -\frac{\alpha(\hat{R}_1 e_1(\theta_e^r) + \hat{R}_2 e_2(\theta_e^r)) (h'_1(\theta_h^r) \hat{R}_1 e_1(\theta_e^r) + h'_2(\theta_h^r) \hat{R}_2 e_2(\theta_e^r))}{(1 + h_1(\theta_h^r) \hat{R}_1 e_1(\theta_e^r) + h_2(\theta_h^r) \hat{R}_2 e_2(\theta_e^r))^2} \quad (\text{C1b})$$

where all  $\hat{R}_i$  are functions of  $\theta_{e,h}^r$ . These entries describe the horizontal and vertical component of the movement vectors in Fig. 5 in the main part and in Fig. E2, respectively. Note that the gradient is independent of the ecological parameter  $r$ . Trait vectors  $\theta_{e,h}^* = (\theta_e^*, \theta_h^*)$  for which the fitness gradient equals zero are called singular points. For symmetry reasons it is clear that  $\theta_{e,h}^* = (0.5, 0.5)$  fulfills this condition.

Around a singular point the second order Taylor expansion of invasion fitness is given by

$$\begin{aligned} w(\theta_{e,h}^m, \theta_{e,h}^*) &\approx \frac{1}{2}(\theta_{e,h}^m - \theta_{e,h}^*)\mathsf{H}(\theta_{e,h}^m - \theta_{e,h}^*)^T \\ &= \frac{1}{2}(h_{11}(\theta_e^m - \theta_e^*)^2 + 2h_{12}(\theta_e^m - \theta_e^*)(\theta_h^m - \theta_h^*) + h_{22}(\theta_h^m - \theta_h^*)^2), \end{aligned} \quad (\text{C2})$$

where  $\mathsf{H} = [h_{ij}]$  is the Hessian matrix of invasion fitness as defined by Eq. (7) in the main part. At the symmetric singular point  $\theta_{e,h}^* = (0.5, 0.5)$  Eqs. (B3) and (B11) are valid. Furthermore,

$$\hat{R}(\theta_{e,h}^*) := \hat{R}_1(\theta_{e,h}^*) = \hat{R}_2(\theta_{e,h}^*) \quad (\text{C3})$$

$$\hat{R}^{(1,0)}(\theta_{e,h}^*) := \hat{R}_1^{(1,0)}(\theta_{e,h}^*) = -\hat{R}_2^{(1,0)}(\theta_{e,h}^*) > 0 \quad (\text{C4})$$

$$\hat{R}^{(0,1)}(\theta_{e,h}^*) := \hat{R}_1^{(0,1)}(\theta_{e,h}^*) = \hat{R}_2^{(0,1)}(\theta_{e,h}^*), \quad (\text{C5})$$

where  $\hat{R}_i^{(1,0)}(\theta_{e,h}^*)$  and  $\hat{R}_i^{(0,1)}(\theta_{e,h}^*)$  indicate differentiation with respect to  $\theta_e^*$  and  $\theta_h^*$ , respectively. With this the Hessian matrix becomes

$$\mathsf{H} = \begin{pmatrix} \frac{2\alpha\hat{R}(\theta_{e,h}^*)e''(\theta_e^*)}{(1+2h(\theta_h^*)\hat{R}(\theta_{e,h}^*)e(\theta_e^*))^2} & -\frac{4\alpha h'(\theta_h^*)\hat{R}(\theta_{e,h}^*)^2e(\theta_e^*)e'(\theta_e^*)}{(1+2h(\theta_h^*)\hat{R}(\theta_{e,h}^*)e(\theta_e^*))^2} \\ -\frac{4\alpha h'(\theta_h^*)\hat{R}(\theta_{e,h}^*)^2e(\theta_e^*)e'(\theta_e^*)}{(1+2h(\theta_h^*)\hat{R}(\theta_{e,h}^*)e(\theta_e^*))^2} & -\frac{4\alpha h''(\theta_h^*)\hat{R}(\theta_{e,h}^*)^2e(\theta_e^*)^2}{(1+2h(\theta_h^*)\hat{R}(\theta_{e,h}^*)e(\theta_e^*))^2} \end{pmatrix}. \quad (\text{C6})$$

Note that the Hessian matrix  $\mathsf{H}$  is independent of the ecological traits  $r$  and  $K$ . In order to ascertain that the singular point  $\theta_{e,h}^*$  is unininvadable,  $\mathsf{H}$  has to be negative definite (both eigenvalues negative). This is the case if and only if its determinant is positive and its trace negative. These conditions can only be evaluated numerically and the green regions in Fig. 5a in the main part and Figs. E3 and E4c indicates when they hold true simultaneously.

From Eqs. (B3) and (B11) follows that the off-diagonal entry of  $\mathsf{H}$  is always positive, implying that the two traits show positive epistatic interactions. A further consequence is that the eigenvector corresponding to the dominant eigenvalue can be chosen such that both entries are positive. Biologically, this means that if the singular point  $\theta_{e,h}^*$  is invadable, then this is most likely to happen through mutants that are specialized in both traits for the same resource as indicated by the grey cones in Fig. 5.

Whether or not the singular point  $\theta_{e,h}^*$  is an attractor of the evolutionary dynamics described by Eq. (6) in the main part depends on the eigenvalues of the matrix  $\mathsf{M}\mathsf{J}$ , where  $\mathsf{M}$  is a symmetric, positive definite variance-covariance matrix and  $\mathsf{J}$  the Jacobian matrix of the selection gradient given by the sum of the Hessian matrix  $\mathsf{H}$  and the matrix  $\mathsf{Q}$  of mixed derivatives

## 8 *The American Naturalist*

---

with respect to both mutant and resident traits (see Eq. 9 in the main part). This matrix equals

$$Q = \begin{pmatrix} \frac{2\alpha\hat{R}^{(1,0)}(\theta_{e,h}^*)e'(\theta_e^*)}{(1+2h(\theta_h^*)\hat{R}(\theta_{e,h}^*)e(\theta_e^*))^2} & 0 \\ -\frac{4\alpha h'(\theta_h^*)\hat{R}^{(1,0)}(\theta_{e,h}^*)e(\theta_e^*)^2}{(1+2h(\theta_h^*)\hat{R}(\theta_{e,h}^*)e(\theta_e^*))^2} & 0 \end{pmatrix}. \quad (C7)$$

Using Eqs. (B3), (B11) and (C4) it follows that both non-zero entries are negative.

Leimar (2009) shows that both eigenvalues of MJ have negative real parts for any variance-covariance matrix M if the symmetric part of the Jacobian, defined as  $J_{\text{sym}} = (J + J^T)/2$ , is negative definite. We refer to this property as strong attractivity. We find

$$J_{\text{sym}} = \begin{pmatrix} \frac{2\alpha(\hat{R}e''(\theta_e^*)+\hat{R}^{(1,0)}e'(\theta_e^*))}{(1+2h(\theta_h^*)\hat{R}e(\theta_e^*))^2} & -\frac{2\alpha h'(\theta_h^*)\hat{R}e(\theta_e^*)(2\hat{R}e'(\theta_e^*)+\hat{R}^{(1,0)}e(\theta_e^*))}{(1+2h(\theta_h^*)\hat{R}e(\theta_e^*))^2} \\ -\frac{2\alpha h'(\theta_h^*)\hat{R}e(\theta_e^*)(2\hat{R}e'(\theta_e^*)+\hat{R}^{(1,0)}e(\theta_e^*))}{(1+2h(\theta_h^*)\hat{R}e(\theta_e^*))^2} & -\frac{4\alpha h''(\theta_h^*)\hat{R}^2e(\theta_e^*)^2}{(1+2h(\theta_h^*)\hat{R}e(\theta_e^*))^2} \end{pmatrix}, \quad (C8)$$

where all  $\hat{R}$ ,  $\hat{R}^{(1,0)}$  and  $\hat{R}^{(0,1)}$  are evaluated at  $\theta_{e,h}^*$ . In the orange and green areas in Fig. 5a in the main part and Figs. E3 and E4c the determinant of  $J_{\text{sym}}$  is positive and its trace is negative, indicating that strong attractivity holds. Thus, for combinations of trade-off curvatures in the orange region in these figures the singular point  $\theta_{e,h}^*$  is both invadable and strongly attracting. Based on the information in the flow-diagram shown in Fig. 3 in the main part we can conclude that it is an evolutionary branching point.

If  $J_{\text{sym}}$  is indefinite, then it is possible that both eigenvalues of MJ have negative real parts for some M but not for others, and if  $J_{\text{sym}}$  is positive definite, then it is guaranteed that  $\theta_{e,h}^*$  is an evolutionary repeller. Using that  $\det(MJ) = \det(M)\det(J)$  and  $\det(M) > 0$ , we also know that the singular point  $\theta_{e,h}^*$  is surely repelling whenever  $\det(J) < 0$  regardless of M since then the real parts of the eigenvalues of MJ have opposite sign. If  $\det(J_{\text{sym}}) < 0$  and  $\det(J) > 0$ , then for the singular point  $\theta_{e,h}^*$  to be an attractor of the evolutionary dynamics for a mutational variance-covariance matrix M with entries  $m_{11}$ ,  $m_{22}$  and  $m_{12}$  it is necessary and sufficient that  $\text{trace}(MJ) < 0$ . This condition can be written as

$$m_{12} > \frac{m_{11}(\hat{R}(\theta_{e,h}^*)e''(\theta_e^*) + \hat{R}^{(1,0)}(\theta_{e,h}^*)e'_1(\theta_e^*)) - 2m_{22}h''(\theta_h^*)\hat{R}(\theta_{e,h}^*)^2e(\theta_e^*)^2}{2h'(\theta_h^*)\hat{R}(\theta_{e,h}^*)e(\theta_e^*)(2\hat{R}(\theta_{e,h}^*)e'(\theta_e^*) + \hat{R}^{(1,0)}(\theta_{e,h}^*)e(\theta_e^*))}, \quad (C9)$$

which implicitly characterizes the set of matrices M for which the singular point  $\theta_{e,h}^*$  is weakly attracting. The yellow regions in Fig. 5a in the main part and Figs. E3 and E4c correspond to combinations of trade-off curves for which  $\det(J_{\text{sym}}) < 0$  and  $\det(J) > 0$ .

Numerical evaluations show that in the yellow region in Fig. 5a the trace of J is negative, implying that the real parts of both eigenvalues of J are negative. With this follows that for M equal to the identity matrix both eigenvalues of MJ have negative real parts and therefore the

singular point is indeed weakly attracting. The same holds true for the upper right yellow region in Fig. E3. Interestingly, there is a second narrow yellow region in the bottom left part of this figure. In this parameter region, the trace of  $J$  is positive, implying that both eigenvalues of  $J$  have positive real parts. Using the function `FindInstance` in Mathematica (Wolfram Research, Inc., 2019) we confirm that also for this region matrices  $M$  exist such that both eigenvalues of  $MJ$  have negative real parts. Obviously, these  $M$  have to be different from the identity matrix.

Next we show that an invadable weakly attracting singular point in Fig. 5a in the main part also fulfills condition (iii) in Fig. 3, namely, that phenotypes that lie on opposite sites of the singular point in the direction in which evolutionary branching is to be expected can coexist in a protected polymorphism. This direction is given by the vector  $z^T = Mu^T$ , where  $u = \{u_1, u_2\}$  is the eigenvector corresponding to the dominant eigenvalue of the Hessian matrix  $H$ . The condition for coexistence is  $-zQz^T > 0$  (Ravigné et al., 2009; Geritz et al., 2016). For  $M$  equal to the identity matrix this condition evaluates to  $u_1(u_1q_{11} + u_2q_{21}) < 0$ . This is always fulfilled given that the non-zero entries of  $Q$  are negative and  $u$  can be chosen such that both entries are positive. Since conditions (ii) and (iii) imply condition (iv) and – for the case of two jointly evolving traits – (iii) also implies (v) (see Fig. 3 in the main part and Geritz et al., 2016) we can conclude that the weakly attracting singular points in the yellow parameter region in Fig. 5a are indeed evolutionary branching points for  $M$  equal to the identity matrix. The same argument can be made for the upper right yellow region in Fig. E3. For the lower left yellow region in Fig. E3 we numerically confirm for selected points that matrices  $M$  exist for which the singular point is weakly attracting and condition (iii) is fulfilled.

Fig. E3 also contains a small region with combinations of trade-off curvatures in which the singular point is weakly attracting and uninvadable. In this parameter region, the singular point is an evolutionary endpoint for  $M$  equal to the identity matrix but an uninvadable evolutionary repellor, sometimes called a *Garden of Eden*-point, for certain other choices of  $M$ .

We conclude by elaborating on the connection between the analyses of singly and jointly evolving traits. The diagonal entries of the matrix  $H$  are equal to Eqs. (B7) and (B13) and the diagonal entries of the matrix  $J$  are equal to Eqs. (B8) and again (B13). If the singular point for one of the singly evolving traits is attracting while the other is repelling, then  $J_{\text{sym}}$  is indefinite and the singular point  $\theta_{e,h}^*$  is either repelling or weakly attracting. Similarly, if the singular point for one of the singly evolving points is invadable while the other is uninvadable, then the Hessian matrix  $H$  is indefinite and the singular point  $\theta_{e,h}^*$  is invadable in some directions but not in others. This follows from the general result for two-dimensional symmetric matrices  $A$  that  $a_{11}a_{22} - a_{12}^2 = \lambda_1\lambda_2$  (e.g. Otto and Day, 2007, p. 238). Applying this result under the above conditions to  $H$  and  $J_{\text{sym}}$  implies that the eigenvalues of these matrices have opposite sign. On the other hand, using the same matrix result it follows that even if both singly evolving traits are attracting (both diagonal entries of  $J$  negative), negative definiteness

of  $J_{\text{sym}}$  is not guaranteed. Similarly, even if both traits are unininvadable when evolving one by one (both diagonal entries of  $H$  negative), unininvadability of  $\theta_{e,h}^*$  is not guaranteed.

## C.2 Joint evolution of conversion efficiency and handling time

Given  $r_1 = r = r_2$ ,  $K_1 = K = K_2$  and  $e_1 = e = e_2$  Eqs. (A1a) and (A1b) simplify to

$$\hat{R}_i(\boldsymbol{\theta}_{\alpha,h}) = \frac{d}{e(\alpha_1(\theta_{\alpha}^r) + \alpha_2(\theta_{\alpha}^r) - d(h_1(\theta_h^r) + h_2(\theta_h^r)))} \quad \text{for } i \in \{1, 2\}. \quad (\text{C10})$$

The selection gradient for joint evolution of  $\alpha$  and  $h$  evaluated at  $\boldsymbol{\theta}_{\alpha,h}^m = \boldsymbol{\theta}_{\alpha,h}^r$  has the entries

$$S_{\alpha}(\boldsymbol{\theta}_{\alpha,h}^r) = \frac{e(\alpha'_1(\theta_{\alpha}^r)\hat{R}_1(\boldsymbol{\theta}_{\alpha,h}^r) + \alpha'_2(\theta_{\alpha}^r)\hat{R}_2(\boldsymbol{\theta}_{\alpha,h}^r))}{1 + e(h_1(\theta_h^r)\hat{R}_1(\boldsymbol{\theta}_{\alpha,h}^r) + h_2(\theta_h^r)\hat{R}_2(\boldsymbol{\theta}_{\alpha,h}^r))} \quad (\text{C11a})$$

$$S_h(\boldsymbol{\theta}_{\alpha,h}^r) = -\frac{e^2(\alpha_1(\theta_{\alpha}^r)\hat{R}_1(\boldsymbol{\theta}_{\alpha,h}^r) + \alpha_2(\theta_{\alpha}^r)\hat{R}_2(\boldsymbol{\theta}_{\alpha,h}^r))(h'_1(\theta_h^r)\hat{R}_1(\boldsymbol{\theta}_{\alpha,h}^r) + h'_2(\theta_h^r)\hat{R}_2(\boldsymbol{\theta}_{\alpha,h}^r))}{(1 + h_1(\theta_h^r)\hat{R}_1(\boldsymbol{\theta}_{\alpha,h}^r)e + h_2(\theta_h^r)\hat{R}_2(\boldsymbol{\theta}_{\alpha,h}^r)e)^2}. \quad (\text{C11b})$$

For symmetry reasons it is clear that  $\boldsymbol{\theta}_{\alpha,h}^* = (\theta_{\alpha}^*, \theta_h^*) = (0.5, 0.5)$  is a singular point. At this singular point Eqs. (B17) and (B11) are valid and we also have  $\hat{R}(\boldsymbol{\theta}_{\alpha,h}^*) := \hat{R}_1(\boldsymbol{\theta}_{\alpha,h}^*) = \hat{R}_2(\boldsymbol{\theta}_{\alpha,h}^*)$ .

The selection Hessian evaluated at the singular point then equals

$$H = \begin{pmatrix} \frac{2\alpha''(\theta_{\alpha}^*)\hat{R}(\boldsymbol{\theta}_{\alpha,h}^*)e}{1+2h(\theta_h^*)\hat{R}(\boldsymbol{\theta}_{\alpha,h}^*)e} & 0 \\ 0 & -\frac{4\alpha(\theta_{\alpha}^*)h''(\theta_h^*)\hat{R}(\boldsymbol{\theta}_{\alpha,h}^*)^2e^2}{(1+2h(\theta_h^*)\hat{R}(\boldsymbol{\theta}_{\alpha,h}^*)e)^2} \end{pmatrix}. \quad (\text{C12})$$

The diagonal entries are identical to Eqs. (B19) and (B13). Importantly, the off-diagonal entries equal zero, implying that epistatic interactions between conversion efficiency  $\alpha$  and handling time  $h$  are absent. Since the eigenvalues of a diagonal matrix are given by its diagonal entries, the singular point  $\boldsymbol{\theta}_{\alpha,h}^m$  is invadable if  $z_{\alpha}$  or  $z_h$  are negative and unininvadable if both are positive.

In order to determine whether or not the singular point  $\boldsymbol{\theta}_{\alpha,h}^m$  is an attractor of the evolutionary dynamics we have to calculate the matrix  $Q$  given by Eq. (9) in the main part. It appears that under our symmetry assumption this matrix is a null matrix. As a consequence, the Jacobian matrix  $J$  is equal to the Hessian matrix,  $J = H$ , and a singular point is an attractor of the evolutionary dynamics if it is unininvadable and a repeller if it is invadable (Fig. E1b) and evolutionary branching is impossible. The same conclusion can be reached by using the theory developed in Metz et al. (2008). For this particular case, one can prove that the trait vector  $\boldsymbol{\theta}_{\alpha,h}^r$  that minimizes (maximizes)  $\hat{R}(\boldsymbol{\theta}_{\alpha,h}^r)$  as given by Eq. (C10) is an unininvadable attractor (invadable repeller).

### C.3 Joint evolution of all three traits

Under the symmetry assumptions  $r_1 = r = r_2$  and  $K_1 = K = K_2$  the selection gradient for joint evolution of all three traits evaluated at  $\theta_{e,h,\alpha}^m = \theta_{e,h,\alpha}^r$  has the entries

$$S_e(\theta_{e,h,\alpha}^r) = \frac{\alpha_1(\theta_\alpha^r)\hat{R}_1 e'_1(\theta_e^r) + \alpha_2(\theta_\alpha^r)\hat{R}_2 e'_2(\theta_e^r) + \hat{R}_1 \hat{R}_2 (\alpha_2(\theta_\alpha^r)h_1(\theta_h^r) - \alpha_1(\theta_\alpha^r)h_2(\theta_h^r))E}{(1 + h_1(\theta_h^r)\hat{R}_1 e_1(\theta_e^r) + h_2(\theta_h^r)\hat{R}_2 e_2(\theta_e^r))^2} \quad (\text{C13a})$$

$$S_h(\theta_{e,h,\alpha}^r) = -\frac{(\alpha_1(\theta_\alpha^r)\hat{R}_1 e_1(\theta_e^r) + \alpha_2(\theta_\alpha^r)\hat{R}_2 e_2(\theta_e^r))(h'_1(\theta_h^r)\hat{R}_1 e_1(\theta_e^r) + h'_2(\theta_h^r)\hat{R}_2 e_2(\theta_e^r))}{(1 + h_1(\theta_h^r)\hat{R}_1 e_1(\theta_e^r) + h_2(\theta_h^r)\hat{R}_2 e_2(\theta_e^r))^2} \quad (\text{C13b})$$

$$S_\alpha(\theta_{e,h,\alpha}^r) = \frac{\alpha'_1(\theta_\alpha^r)\hat{R}_1 e_1(\theta_e^r) + \alpha'_2(\theta_\alpha^r)\hat{R}_2 e_2(\theta_e^r)}{1 + h_1(\theta_h^r)\hat{R}_1 e_1(\theta_e^r) + h_2(\theta_h^r)\hat{R}_2 e_2(\theta_e^r)}, \quad (\text{C13c})$$

where all  $\hat{R}_i$  are functions of  $\theta_{e,h,\alpha}^r$  and  $E = e_1(\theta_e^r)e'_2(\theta_e^r) - e'_1(\theta_e^r)e_2(\theta_e^r)$ . For symmetry reasons it is clear that the symmetric strategy  $\theta_{e,h,\alpha}^* = (\theta_e^*, \theta_h^*, \theta_\alpha^*) = (0.5, 0.5, 0.5)$  is a singular point.

The entries of three-dimensional Hessian matrix  $H$  are available from the Hessian matrices of the three cases of pairwise evolving traits. The singular point  $\theta_{e,h,\alpha}^*$  is unininvadable if the Hessian matrix is negative definite. Note, that the definiteness of the three-dimensional Hessian cannot be inferred form the definiteness of the three two-dimensional Hessian matrices. The green surface in Fig. 6 in the main part shows where  $\det(H)$  changes sign, which indicates where  $H$  changes from negative definite to indefinite.

Next we determine the Jacobian matrix  $J$  of the selection gradient and its symmetric part  $J_{\text{sym}}$ , the entries of which are available from the Jacobian matrices and their symmetric parts, respectively, of the three cases of pairwise evolving traits. The singular point  $\theta_{e,h,\alpha}^*$  is an attractor of the evolutionary dynamics given by Eq. (6) in the main part independent of the three-dimensional mutational variance-covariance matrix  $M$  (i.e., strongly attracting) if  $J_{\text{sym}}$  is negative definite. The orange surface in Fig. 6 shows where  $\det(J_{\text{sym}})$  changes sign, which indicates where  $J_{\text{sym}}$  changes from negative definite to indefinite.

More generally, the singular point  $\theta_{e,h,\alpha}^*$  is an attractor of the evolutionary dynamics given by Eq. (6) if all eigenvalues of the matrix  $MJ$  have negative real parts. If  $J_{\text{sym}}$  is indefinite, then it is possible that all eigenvalues of  $MJ$  have negative real parts for some  $M$  but not for others (weak attractivity). The Routh-Hurwitz criterion (e.g. Otto and Day, 2007, p. 310) states that for the case of three jointly evolving traits  $\det(MJ) < 0$  is necessary for all eigenvalues to have negative real parts. Since  $\det(MJ) = \det(M)\det(J)$  and  $\det(M) > 0$  the sign of  $\det(MJ)$  is given by the sign of  $\det(J)$ . Combinations of trade-off curvature parameters at which  $\det(J)$  changes sign are therefore informative about changes in the sign of the real parts its eigenvalues. If all eigenvalues have negative real parts (such that  $\det(J) < 0$ ) for trade-off curvature parameters on one side of a manifold defined by  $\det(J) = 0$ , then generically one eigenvalue has a positive real part and two a negative real part for parameters on the other side of this manifold (such that  $\det(J) > 0$ ). In the latter case, it is guaranteed that  $\theta_{e,h,\alpha}^*$  is

## 12 *The American Naturalist*

---

an evolutionary repeller. For our model, the manifold at which  $\det(J)$  changes sign is very close to the boundary where  $\det(J_{\text{sym}})$  changes sign. Thus, the parameter region where the singular point can potentially be weakly attracting is very narrow and therefore omitted from Fig. 6 for clarity. For Fig. 6 we nevertheless confirm numerically that for combinations of trade-off curvatures for which  $\det(J_{\text{sym}}) > 0$  and  $\det(J) < 0$  the matrix  $J$  also fulfills the other two Routh-Hurwitz criteria. Thus, in the parameter region of potentially weakly attracting singular points indeed all eigenvalues of  $J$  have negative real parts. With this we can conclude that the identity matrix serves as a matrix  $M$  for which the singular point is indeed an attractor of the evolutionary dynamics.

Fig. 3 in the main part indicates that at a strongly attracting and invadable singular point also condition (iii) and (iv) are fulfilled but that condition (v) has to be evaluated independently. This condition is fulfilled if the two strategies emerging at an evolutionary branching point diverge faster than the mean of their strategy values changes. This is the case if the dominant eigenvalues of the matrix  $(I + 1/2Qu^T u)J$  is less than the dominant eigenvalue of the Hessian matrix (Geritz et al., 2016). Here,  $I$  is the three-dimensional identity matrix and  $u$  is the right eigenvector of  $H$  normalized such that  $uQu^T = -2$ . A numerical evaluation of this condition for combinations of trade-off curvatures resulting in strongly attracting and invadable singular points confirms that (v) indeed holds true (see Mathematica notebook deposited in the Dryad Digital Repository: <https://doi.org/10.5061/dryad.ns1rn8pnf>, Vasconcelos and Rueffler, 2019). Thus, the strongly attracting and invadable singular points in Fig. 6 are indeed evolutionary branching points.

As was the case for feeding efficiency evolving jointly with handling time, for weakly attracting and invadable singular points  $\theta_{e,h,\alpha}^*$  condition (iii) has to be evaluated independently. For  $M$  equal to the identity matrix the condition  $-uQu^T > 0$  evaluates to  $u_1q_{11} + u_2q_{21} + u_3q_{31} < 0$ , which is always fulfilled given that the non-zero entries of  $Q$  are negative and  $u$  can be chosen such that all entries are positive. The latter follows from Rayleigh's theorem (e.g. Horn and Johnson, 2013, p. 234) by noting that all off-diagonal entries of  $H$  are non-negative. For various combinations of trade-off curvatures resulting in weakly attracting and invadable singular points, condition (v) is again confirmed numerically, indicating that these singular points are indeed also evolutionary branching points.

## D Individual-based simulations

To explore the robustness of our predictions based on the adaptive dynamics approximation we perform individual-based simulations that relax the assumptions of infinite population size and strict separation of the ecological and evolutionary time scales. The results are shown in Figs. D1-D4 and we here describe the procedure. Simulations were performed in MATLAB (The MathWorks, Inc., 2017) and the code is deposited in the Dryad Digital Repository: <https://doi.org/10.5061/dryad.ns1rn8pnf> (Vasconcelos and Rueffler, 2019).

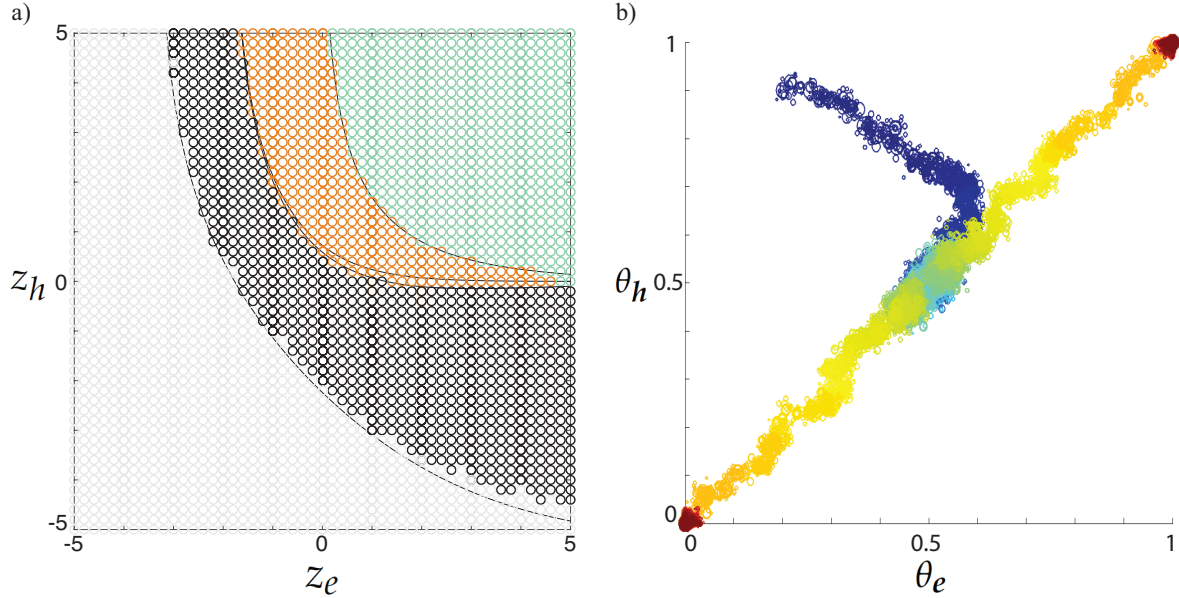


Figure D1: (a) Bifurcation diagram derived from individual-based simulations delimiting different evolutionary outcomes based on trade-off curvature parameters  $z_e$  (x-axis) and  $z_h$  (y-axis). Each dot gives the result from a single simulation run. Gray dots correspond to trade-off combinations that result in non-viable consumer populations. Further colors indicate the evolutionary behavior of the singular point  $\theta_{e,h}^* = (0.5, 0.5)$ : black - invadable repeller, orange - invadable and attracting (i.e. branching point), green - uninadable and attracting. Curves give the expected boundaries between these regions based on the analytical results presented in Fig. 5a in the main part. (b) Simulation run showing the evolutionary trajectory in trait space given the trade-off curvature parameters  $z_e = z_h = 1$  and the initial population trait vector  $(\theta_e, \theta_h) = (0.2, 0.9)$ . Colors indicate the passage of time, whereby blue corresponds to  $t = 0$  and red to  $t = 5 \times 10^5$ . Other parameter values as in Fig. 5a and  $r_1 = 1000 = r_2$ ,  $M = \{\{0.0001, 0\}, \{0, 0.0001\}\}$ .

In order to simplify the simulation procedure, we discretize the continuous time model given by Eq. (1) in the main part as follows. We assume that resources live on a faster time scale than consumers such that the resources reach a quasi-equilibrium within a single consumer generation. We denote the faster time scale of the resources with  $\tau$  and the slow time scale of the consumers with  $t$ . In the presence of  $n$  consumer genotypes  $\theta_{e,h,a}^i$  ( $i \in \{1, \dots, n\}$ ) with densities  $C^i(t)$  at time  $t$  the dynamics of the resources is given by

$$\frac{dR_1}{d\tau} = r_1 R_1(\tau) \left( 1 - \frac{R_1(\tau)}{K_1} \right) - \sum_{i=1}^n \frac{R_1(\tau) e_1(\theta_e^i) C^i(t)}{1 + h_1(\theta_h^i) R_1(\tau) e_1(\theta_e^i) + h_2(\theta_h^i) R_2(\tau) e_2(\theta_e^i)} \quad (\text{D1a})$$

$$\frac{dR_2}{d\tau} = r_2 R_2(\tau) \left( 1 - \frac{R_2(\tau)}{K_2} \right) - \sum_{i=1}^n \frac{R_2(\tau) e_2(\theta_e^i) C^i(t)}{1 + h_1(\theta_h^i) R_1(\tau) e_1(\theta_e^i) + h_2(\theta_h^i) R_2(\tau) e_2(\theta_e^i)}. \quad (\text{D1b})$$

These equations are solved numerically for their quasi-equilibrium  $\hat{R}_1(t)$  and  $\hat{R}_2(t)$  as determined by the consumer densities at time  $t$ . The dynamics of the  $n$  consumer genotypes is given by

$$C^i(t+1) = C^i(t) + C^i(t) \frac{\alpha_1(\theta_\alpha^i)\hat{R}_1(t)e_1(\theta_e^i) + \alpha_2(\theta_\alpha^i)\hat{R}_2(t)e_2(\theta_e^i)}{1 + h_1(\theta_h^i)\hat{R}_1(t)e_1(\theta_e^i) + h_2(\theta_h^i)\hat{R}_2(t)e_2(\theta_e^i)} - C^i(t)d. \quad (\text{D2})$$

The second and third term on the right-hand side equal the number of offspring and the number of death for genotype  $i$ , respectively. For each genotype  $i$  we determine the total number of offspring by drawing a random number from a Poisson distribution with a mean given by the second term on the right-hand side of Eq. (D2) and the number of consumer death by drawing a random number from a binomial distribution where the number of trials is the number of consumer individuals of genotype  $i$  and the death probability  $d$  is the probability of success.

To determine the number of mutants among the offspring of each genotype we draw a random number from a binomial distribution where the number of trials is the number of offspring, and the probability of success is the *per capita* mutation probability  $\mu = 0.0005$ . The trait vector of mutant individuals is determined by drawing a random vector from a – depending on the number of jointly evolving traits – two- or three-dimensional Gaussian distribution with a mean equal to the individual's parent's trait vector. The Gaussian distribution has the variances  $\text{var}(x) = 0.0001$  and for Figs. D1 and D2 the covariance  $\text{cov}(x, y) = 0$  for  $x, y \in \{\theta_e, \theta_h, \theta_\alpha\}$ . For Fig. D3 the covariance  $\text{cov}(\theta_e, \theta_h)$  is as specified in the legend.

Figs. D1a and D2 show the analogues of Figs. 5a and 6 in the main part as derived from simulations at  $51 \times 51 = 2601$  and  $21 \times 21 \times 21 = 9261$ , respectively, combinations of trade-off curvature parameters. For each combination the dynamics is simulated for 1 million consumer generations (unless the consumer population went extinct, in which case the simulation is aborted) starting from a monomorphic population with trait vectors  $(\theta_e, \theta_h) = (0.35, 0.35)$  and  $(\theta_e, \theta_h, \theta_\alpha) = (0.35, 0.35, 0.35)$ , respectively. At the end of the simulation the outcome is determined as follows. A singular point is classified as an evolutionary branching point if at least 35% of the consumer individuals had a trait vector  $(\theta_e, \theta_h) > (0.6, 0.6)$  ( $(\theta_e, \theta_h, \theta_\alpha) > (0.6, 0.6, 0.6)$ ) and another 35% had a trait vector  $(\theta_e, \theta_h) < (0.4, 0.4)$  ( $(\theta_e, \theta_h, \theta_\alpha) < (0.4, 0.4, 0.4)$ ). This means that at least 70% of the population has diverged into two clearly separated clusters. A singular point is classified as an evolutionary repeller if the trait vectors of at least 95% of the individuals fulfilled  $(\theta_e, \theta_h) > (0.6, 0.6)$  ( $(\theta_e, \theta_h, \theta_\alpha) > (0.6, 0.6, 0.6)$ ) or  $(\theta_e, \theta_h) < (0.4, 0.4)$  ( $(\theta_e, \theta_h, \theta_\alpha) < (0.4, 0.4, 0.4)$ ). Finally, a singular point is classified as an evolutionary endpoint (both attracting and uninvadable) if the trait vector of all individuals fulfilled  $(0.4, 0.4) < (\theta_e, \theta_h) < (0.6, 0.6)$  ( $(0.4, 0.4, 0.4) < (\theta_e, \theta_h, \theta_\alpha) < (0.6, 0.6, 0.6)$ ). Comparing Fig. D1a and D2 with Fig. 5a and 6, respectively, shows that the simulations confirm our analytical predictions.

Fig. D4 shows individual simulation runs where it is assumed that mutations affect either only  $\theta_e$  or  $\theta_h$ . In a first step, it is determined which of the two traits is affected by a mutation, where it is assumed that both traits mutate with equal probability. In a second step, a random number is drawn from a one-dimensional Gaussian distribution with a mean equal to the individual's parent's value for the mutating trait and the variance  $var(x) = 0.0001$ . In these simulations, we increase the intrinsic growth rate of the resources from  $r_1 = 1000 = r_2$  (first row in Fig. D4) to  $r_1 = 10000 = r_2$  (second row in Fig. D4), resulting in approximately  $\sim 1300$  and  $\sim 13000$  consumer individuals, respectively. These simulations suggest that the final outcome of the evolutionary dynamics does not require mutations affecting both traits simultaneously.

## References

- Geritz, S. A. H., É. Kisdi, G. Meszéna, and J. A. J. Metz. 1998. Evolutionarily singular strategies and the adaptive growth and branching of the evolutionary tree. *Evolutionary Ecology* 12:35–57.
- Geritz, S. A. H., J. A. J. Metz, and C. Rueffler. 2016. Mutual invadability near evolutionarily singular strategies for multivariate traits, with special reference to the strongly convergence stable case. *Journal of Mathematical Biology* 72:1081–1099.
- Horn, R., and C. Johnson. 2013. *Matrix Analysis*. 2nd ed. Cambridge University Press.
- Iannelli, M., and A. Pugliese. 2014. *An Introduction to Mathematical Population Dynamics*. Springer.
- Leimar, O. 2009. Multidimensional convergence stability. *Evolutionary Ecology Research* 11:191–208.
- Metz, J. A. J. 2008. Fitness. Pages 1599–1612 in S. Jørgensen and B. Fath, eds. *Evolutionary Ecology*. Vol. [2] of *Encyclopedia of Ecology*. Elsevier.
- Metz, J. A. J., S. D. Mylius, and O. Diekmann. 2008. When does evolution optimise? *Evolutionary Ecology Research* 10:629–654.
- Metz, J. A. J., R. M. Nisbet, and S. A. H. Geritz. 1992. How should we define 'fitness' for general ecological scenarios? *Trends in Ecology and Evolution* 7:198–202.
- Otto, S. P., and T. Day. 2007. *A Biologist's Guide to Mathematical Modeling in Ecology and Evolution*. Princeton University Press, Princeton, NJ.
- Ravigné, V., U. Dieckmann, and I. Olivieri. 2009. Live where you thrive: Joint evolution of habitat choice and local adaptation facilitates specialization and promotes diversity. *The American Naturalist* 174:E141–E169.
- The MathWorks, Inc. 2017. Matlab r2017a. Natick, MA, USA.
- Vasconcelos, P., and C. Rueffler. 2019. Code files for: How does joint evolution of consumer traits affect resource specialization? Dryad Digital Repository <https://doi.org/10.5061/dryad.ns1rn8pnf>.
- Wolfram Research, Inc. 2019. Mathematica, Version 12.0.

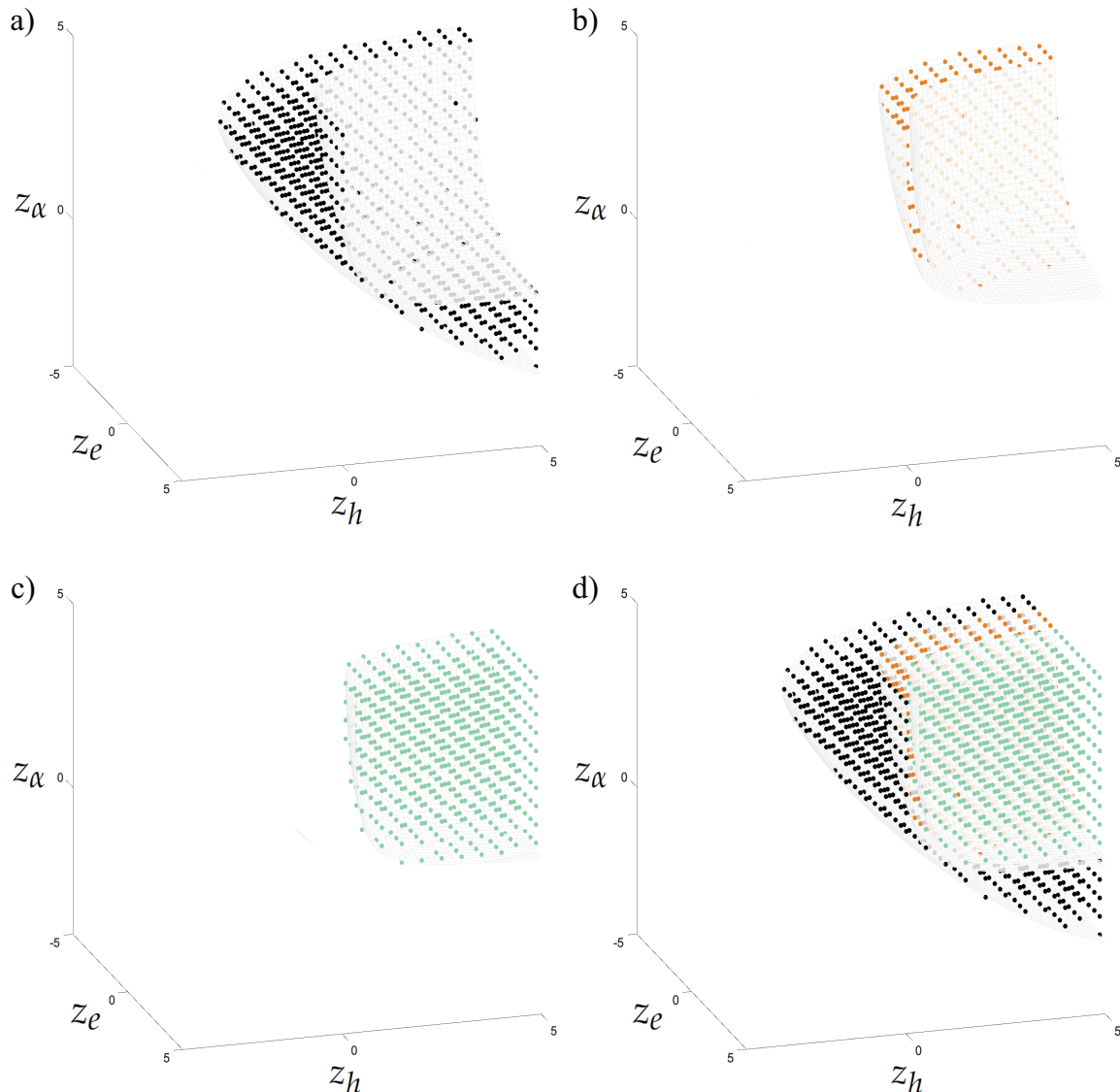


Figure D2: Bifurcation diagram derived from individual-based simulations delimiting different evolutionary outcomes based on trade-off curvature parameters  $z_h$  (x-axis),  $z_\alpha$  (y-axis) and  $z_e$  (z-axis). Each dot gives the result from a single simulation run. Colors indicate the evolutionary behavior of the singular point  $\theta_{e,h,\alpha}^* = (0.5, 0.5, 0.5)$ . (a) Black dots: invadable repelling singular points, delimited by the extinction boundary surface to the left and the surface where the symmetric part of the Jacobian matrix  $J_{\text{sym}}$  changes from indefinite to negative definite to the right. (b) Orange dots: invadable and strongly attracting singular points (i.e. branching points), delimited by the surface where  $J_{\text{sym}}$  changes from indefinite to negative definite to the left and the surface where the Hessian matrix  $H$  changes from indefinite to negative definite to the right. (c) Green dots: uninvadable and attracting singular points, delimited by the surface where  $H$  changes from indefinite to negative definite to the left. In (d) the information from (a)-(c) is combined in a single figure. Other parameters as in Fig. 6 in the main part and  $r_1 = 1000 = r_2$ .

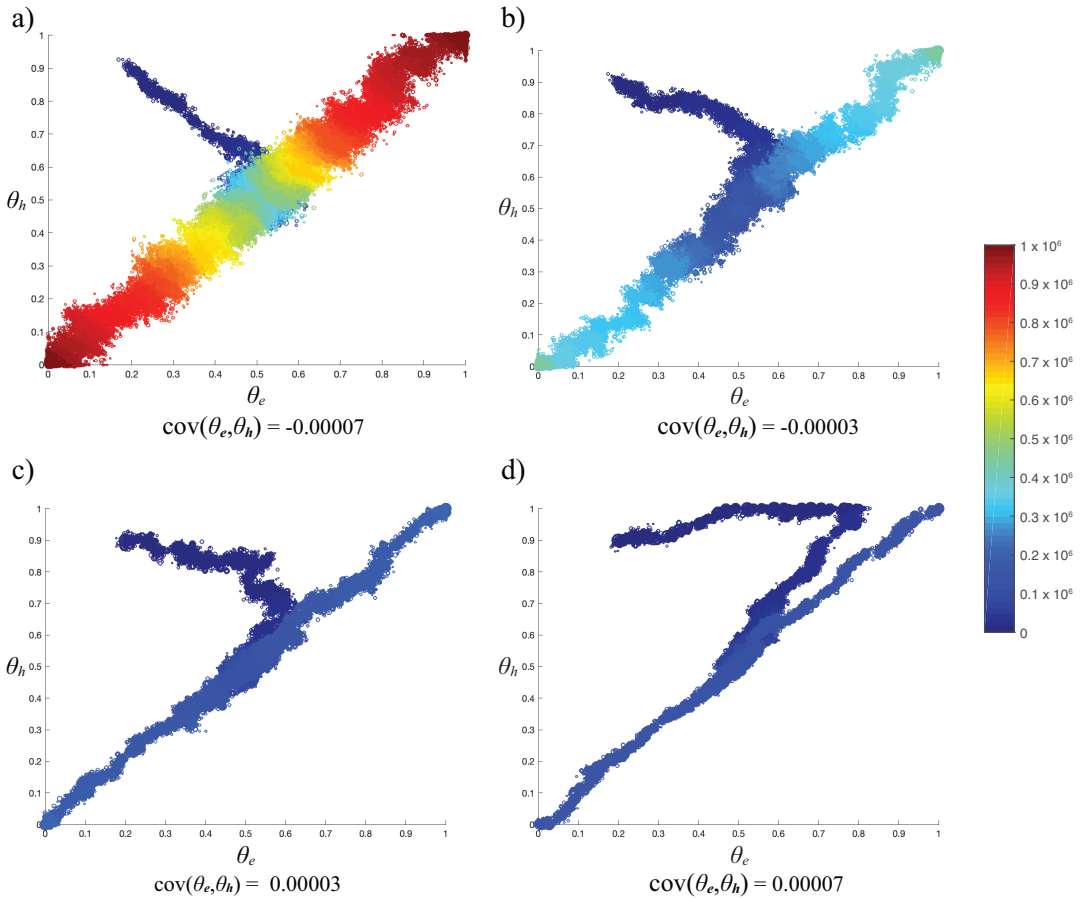


Figure D3: Simulation runs showing the evolutionary trajectory in trait space for the same parameters as in Fig. D1b but with different mutational variance-covariance matrices. In all panels the mutational variances (i.e., the diagonal entries in  $M$ ) are  $m_{11} = 0.0001 = m_{22}$ . The covariance (i.e., the off-diagonal entry in  $M$ ) varies as follows: (a)  $m_{12} = -0.00007$ , (b)  $m_{12} = -0.00003$ , (c)  $m_{12} = 0.00003$ , and (d)  $m_{12} = 0.00007$ . Colors indicate the passage of time, whereby dark blue corresponds to  $t = 0$  and dark red to  $t = 1 \times 10^6$ . The following observations can be made. First, increasing the mutational correlation changes the trajectory toward the singular point from straight to increasingly curved. This should be compared with the trajectory in the absence of mutational correlations in Fig. D1b and the deterministic trajectory in Fig. 5e in the main part. Second, the time for evolutionary branching to occur and the amount of genetic variation in each of the diverging clusters decreases as mutational correlations increase from negative to positive. Third, the final outcome of the evolutionary dynamics is independent of  $m_{12}$ . Other parameter values as in Fig. 5a and  $r_1 = 1000 = r_2$ .

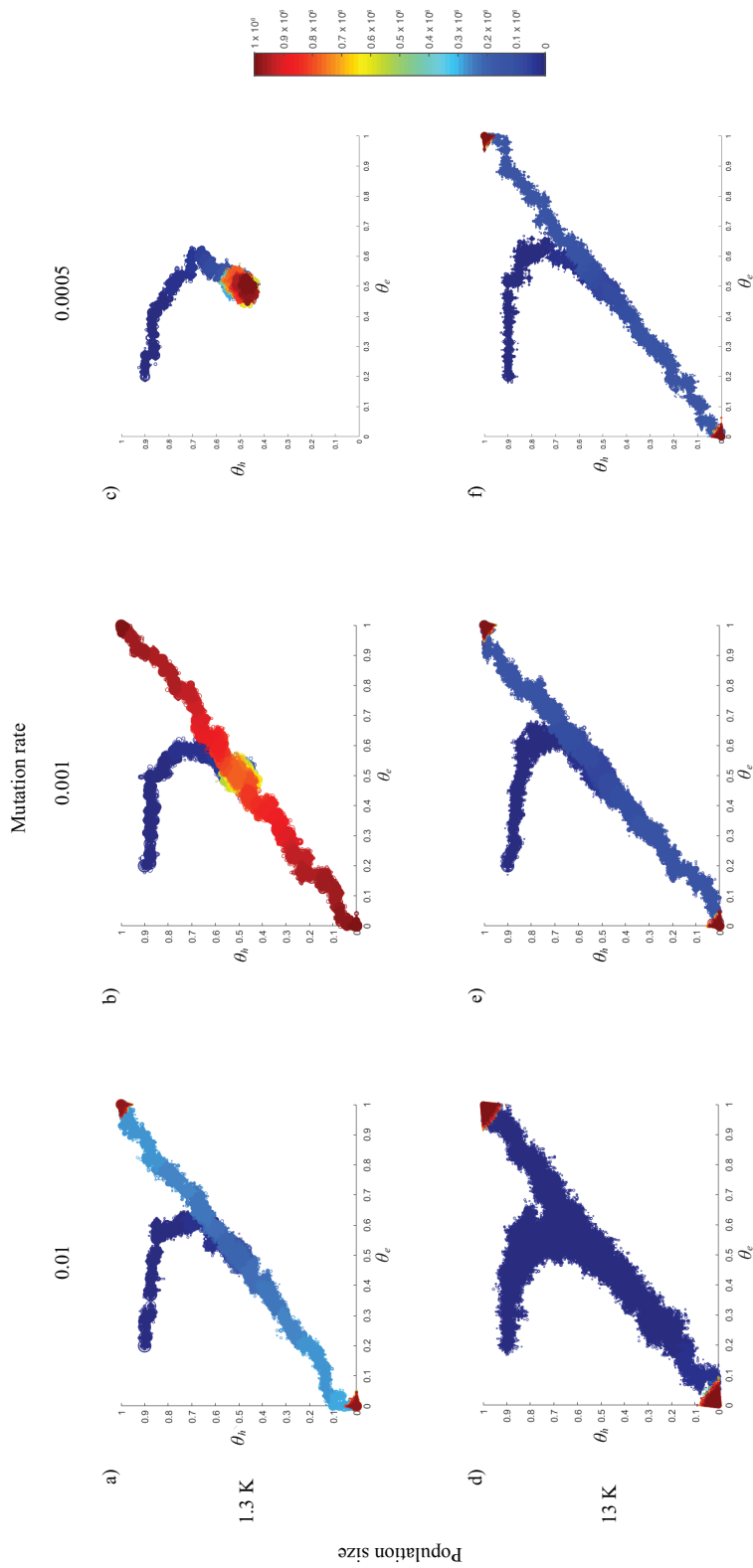


Figure D4: Simulation runs as in Fig. D1b showing the evolutionary trajectory in trait space given the trade-off curvature parameters  $z_e = 1 = z_h$  but for a different mutation process in which each mutation affects either only  $e$  or  $h$ . Simulations are shown for three different *per capita* mutation probabilities  $\mu$  (columns) and two different values of  $r_1 = r_2$ , namely,  $r_1 = 1000 = r_2$  in the first row and  $r_1 = 10000 = r_2$  in the second row, resulting in approximately 1300 and 13000 consumer individuals, respectively. The final outcome of the evolutionary dynamics is identical to that in Figs. D1b and D3 except for the combination of small population size and rare mutations. For this parameter combination, population divergence has not yet occurred by the end of the simulation. Colors indicate the passage of time, whereby blue corresponds to  $t = 0$  and red to  $t = 5 \times 10^5$ . Other parameter values as in Fig. 5a in the main part.

## E Appendix: Additional Figures

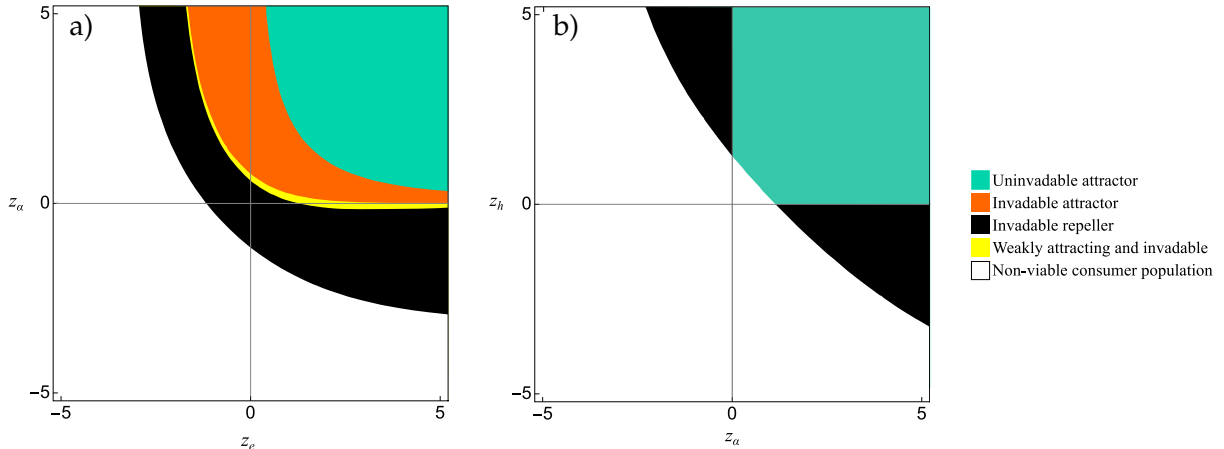


Figure E1: (a) Joint evolutionary dynamics of feeding efficiency  $e$  and conversion efficiency  $\alpha$ . Bifurcation diagram of the singular point  $\theta_{e,\alpha}^* = (0.5, 0.5)$  delimiting different evolutionary outcomes based on trade-off curvature parameters  $z_e$  (x-axis) and  $z_\alpha$  (y-axis). (b) Joint evolutionary dynamics of conversion efficiency  $\alpha$  and handling time  $h$ . Bifurcation diagram of the singular point  $\theta_{\alpha,h}^* = (0.5, 0.5)$  delimiting different evolutionary outcomes based on trade-off curvature parameters  $z_\alpha$  (x-axis) and  $z_h$  (y-axis). Other parameters:  $K_1 = 2.5 = K_2$ ,  $d = 0.9$ , (a)  $h_1 = 0 = h_2$ , (b)  $e_1 = 1 = e_2$ .

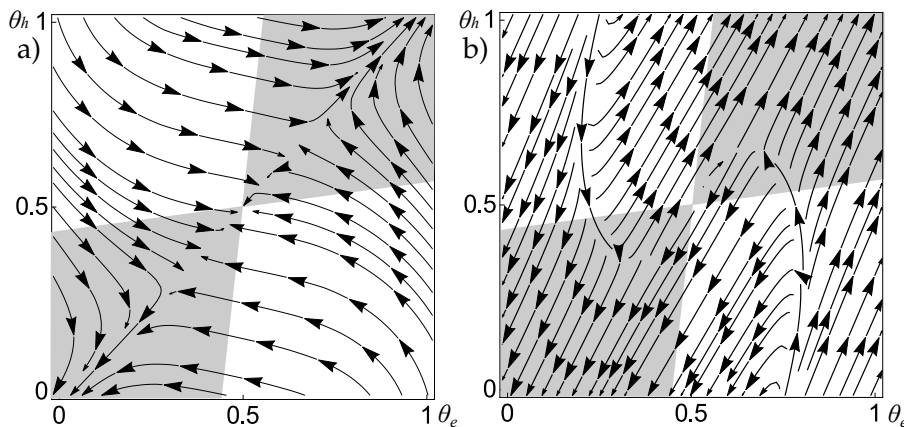


Figure E2: Phase-plane diagrams of the joint evolutionary dynamics of feeding efficiency  $e$  (x-axis) and handling time  $h$  (y-axis) for  $z_e = 0.4 = z_h$  for two different mutational variance-covariance matrices  $M$ . This combination of trade-off curvatures lies in the yellow region in Fig. 5a in the main part and therefore results in a weakly attracting singular point. (a)  $M = \{\{1, 0\}, \{0, 1\}\}$ . This results in the singular point  $\theta_{e,h}^* = (0.5, 0.5)$  being a local attractor that is accompanied by two repelling singular points. Since the symmetric singular point is also invadable it is an evolutionary branching point. (b)  $M = \{\{0.25, 0.47\}, \{0.47, 1\}\}$ . This results in the singular point  $\theta_{e,h}^* = (0.5, 0.5)$  being an evolutionary repeller. Other parameters as in Fig. 5a.

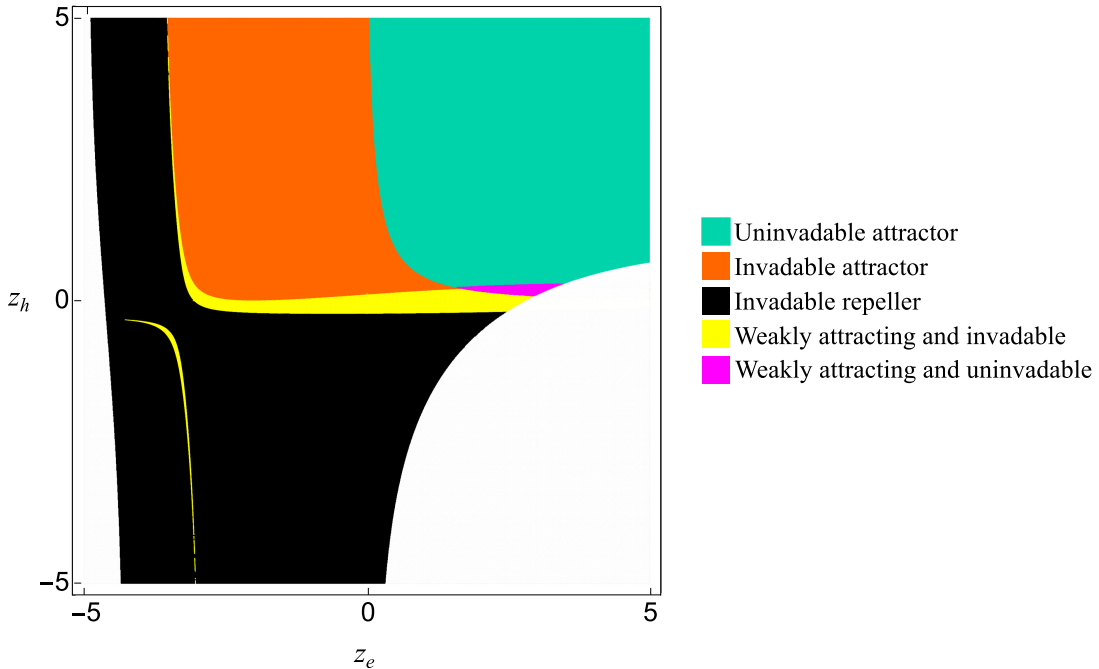


Figure E3: Bifurcation diagram delimiting different evolutionary outcomes for the joint evolutionary dynamics of feeding efficiency  $e$  and handling time  $h$ . This figure is analogous to Fig. 5a in the main part but based on a different set of parameters, namely:  $K_1 = 1.6 = K_2$ ,  $d = 0.3$  and  $\alpha_1 = 1.2 = \alpha_2$ . This bifurcation diagram contain three features not present in Fig. 5a. First, there exists a small set of trade-off curvature parameters in which the singular point  $\theta_{e,h}^*$  is weakly attracting and uninvadable (purple region). In this region, the singular point is an endpoint of evolution for, e.g.,  $M = \{\{1,0\}, \{0,1\}\}$  while it is an uninvadable repeller (also known as "Garden of Eden") for certain other  $M$ . Second, there exists a small and isolated set of trade-off curvature parameters in which the singular point is weakly attracting and invadable (yellow region in the bottom left). The difference between the two yellow regions is that in the top-right yellow region both eigenvalues of the Jacobi matrix  $J$  have positive real parts while in the bottom-left yellow region both eigenvalues of  $J$  have negative real parts. In both regions, mutational variance-covariance matrices  $M$  exists such that both eigenvalues of the matrix  $MJ$  have negative real parts. In the first case, the identity matrix serves this purpose while in the second case  $M$  has to be a matrix with non-zero off-diagonal entries. In the black region separating the two yellow regions the Jacobi matrix  $J$  has one positive and one negative eigenvalue and in the black region to the left of the bottom-left yellow region the symmetric part of the Jacobi matrix,  $J_{\text{sym}}$ , is positive definite. Third, for weak trade-offs in  $e$  combined with strong trade-offs in  $h$  the population dynamical equilibrium of Eq. (1) in the main part, given by Eq. (A2), is unstable (gray region). In this study, we restrict our evolutionary analysis to stable population dynamical equilibria.

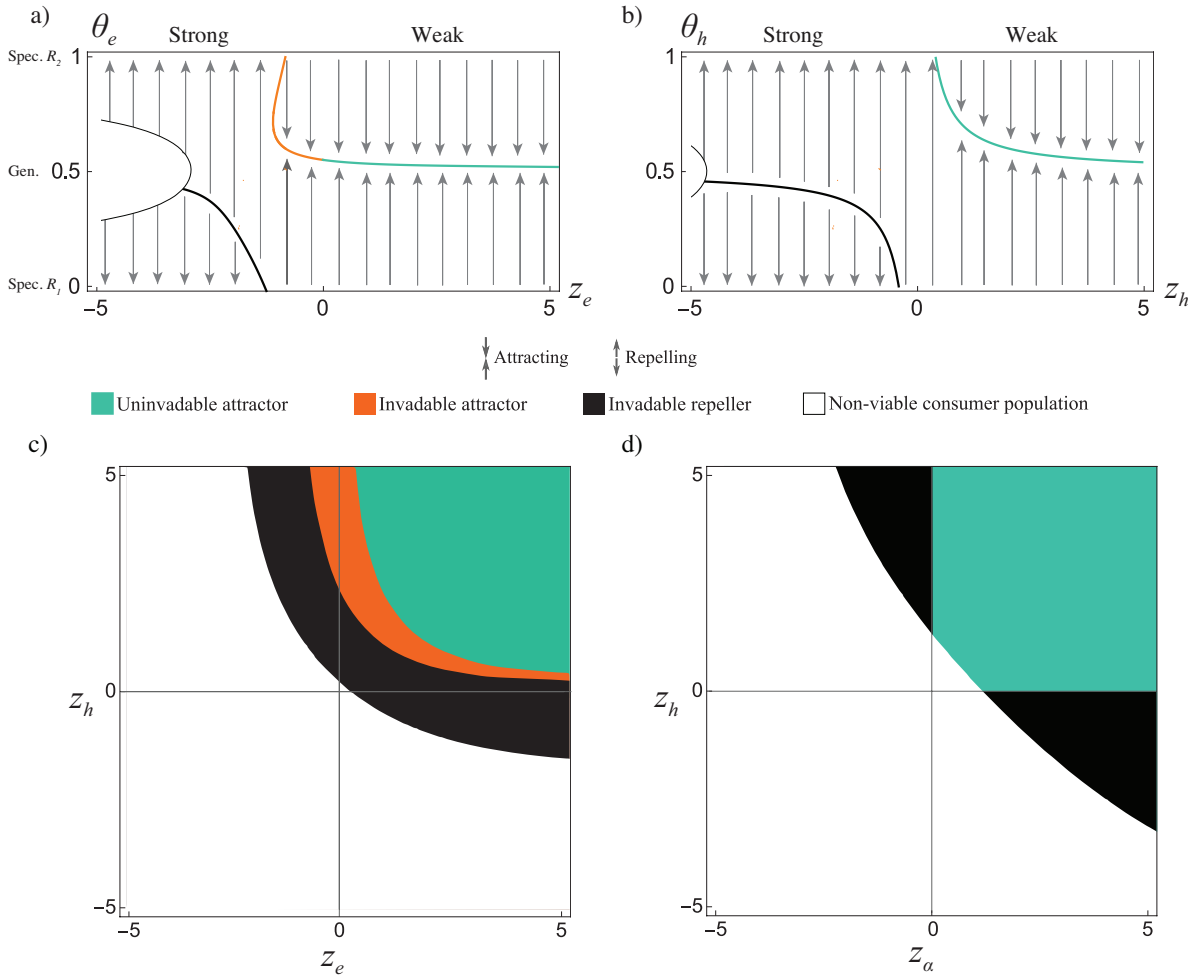


Figure E4: Evolutionary dynamics for asymmetric carrying capacity values  $K_1 = 2$  and  $K_2 = 3$ . All other parameter values are as in the corresponding figures with the symmetric carrying capacity values  $K_1 = 2.5 = K_2$ . (a) Bifurcation diagram for feeding efficiency  $e$  and (b) handling time  $h$  analogous to Fig. 4a,b in the main part. (c) Bifurcation diagram for the joint evolutionary dynamics of feeding efficiency  $e$  and handling time  $h$  analogous to Fig. 5a in the main part. Note that in this panel the parameter region resulting in weak attractivity is very narrow and omitted for clarity. (d) Bifurcation diagram for the joint evolutionary dynamics of conversion efficiency  $\alpha$  and handling time  $h$  analogous to Fig. E1b. These figures show that the results derived under full symmetry are not affected qualitatively by moderate asymmetries.

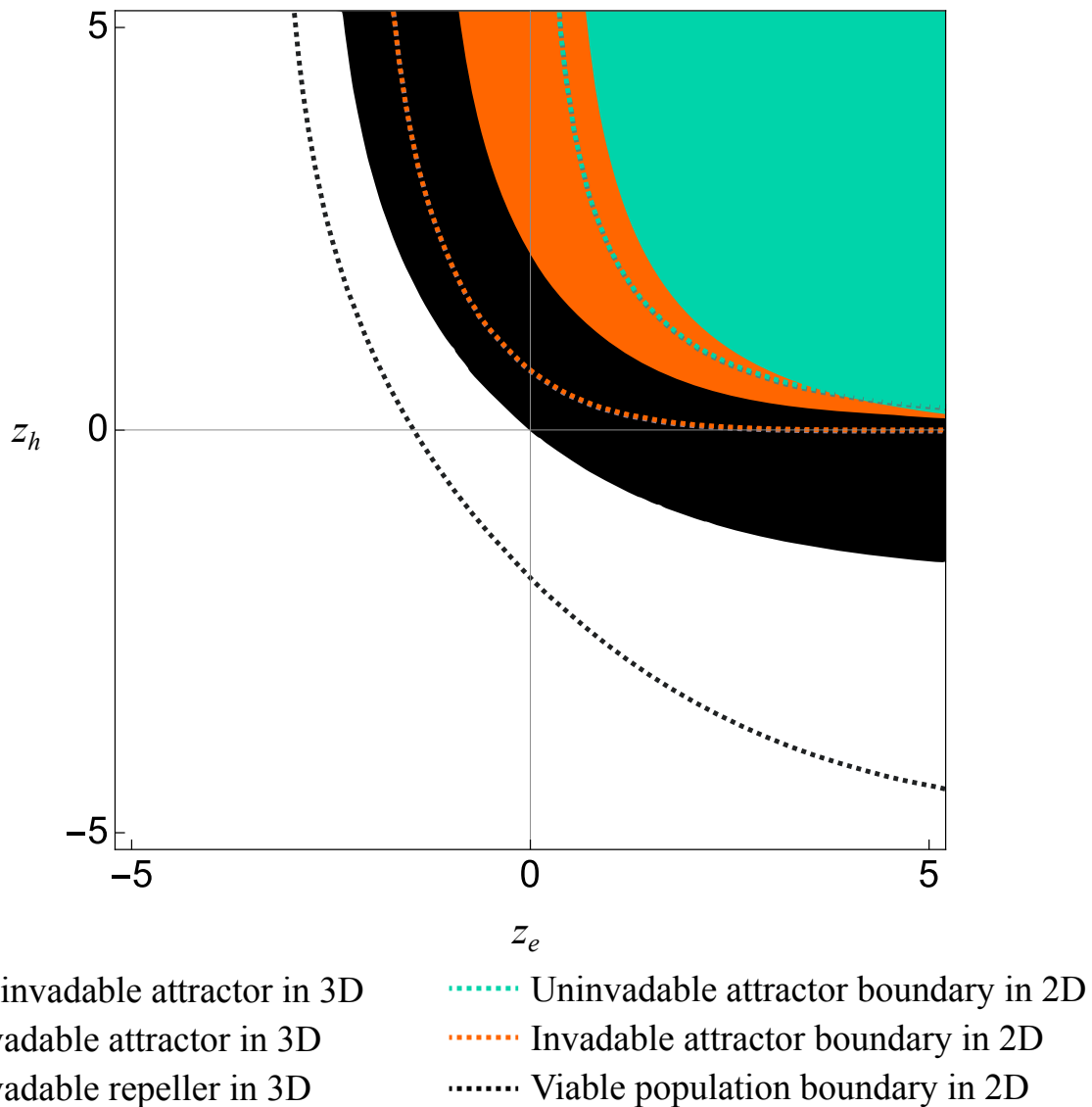


Figure E5: Comparison between the joint evolution of feeding efficiency  $e$  and handling time  $h$  and the joint evolution of all three traits for the same parameters as in Fig. 6 in the main part. Colored surfaces indicate different evolutionary properties of the singular point  $\theta_{e,h,\alpha}^* = (0.5, 0.5, 0.5)$  as a function of the trade-off curvature parameters  $z_e$  (x-axis) and  $z_h$  (y-axis) and  $z_\alpha = 5$ . Thus, the colored areas correspond to the top surface of the cube in Fig. 6. Dotted lines give the boundaries between different evolutionary behaviors at the singular point  $\theta_{e,h}^* = (0.5, 0.5)$  given that the then fixed parameter values  $\alpha_1$  and  $\alpha_2$  are calculated from Eq. (2) in the main part using  $z_\alpha = 5$ . The comparison shows that the values of  $z_e$  and  $z_h$  that allow for evolutionary branching under joint evolution of three traits are shifted toward higher values compared to the case of two jointly evolving traits. Note that the narrow region in which the singular point is weakly attracting is omitted for clarity.

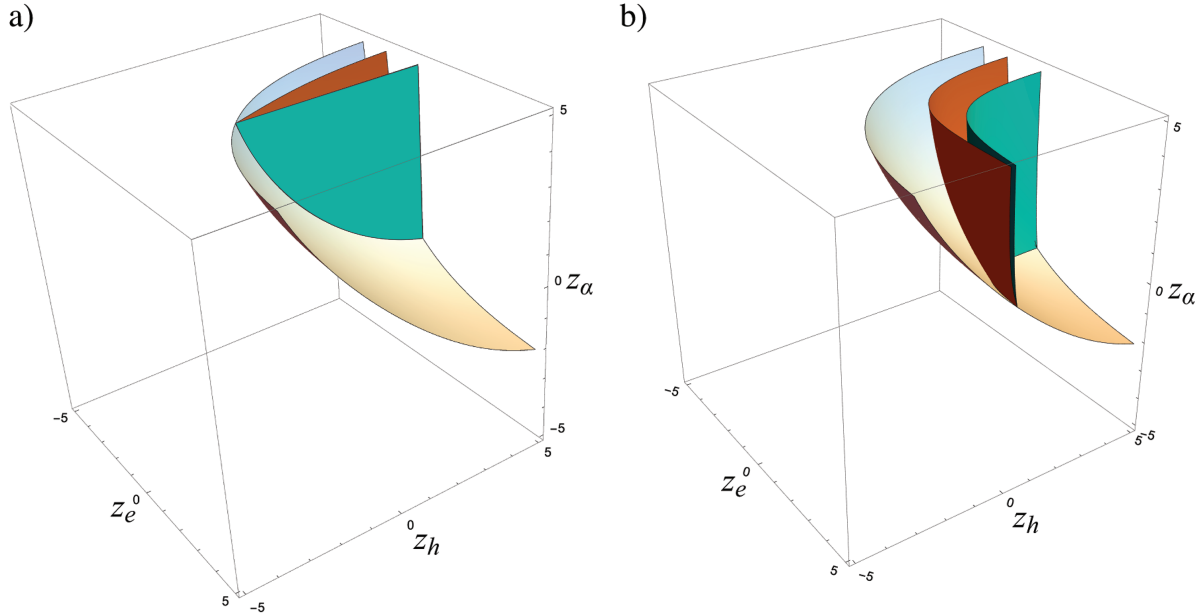


Figure E6: Evolutionary dynamics of (a) feeding efficiency  $e$  and (b) feeding efficiency  $e$  jointly with handling time  $h$  based on the trade-off curvature parameters  $z_h$  (x-axis),  $z_\alpha$  (y-axis) and  $z_e$  (z-axis). The values of the non-evolving traits  $\alpha$  and  $h$  in (a) and  $\alpha$  in (b) are determined by Eqs. (2) and (3) in the main part, respectively, with  $\theta_\alpha = 0.5$ ,  $\alpha_{1\max} = 1 = \alpha_{2\max}$  and  $\theta_h = 0.5$ ,  $h_{1\max} = 1 = h_{2\max}$ ,  $h_{1\min} = 1 = h_{2\min}$ , respectively, and trade-off curvature parameter values as given on the corresponding axes. Colored surfaces have the same meaning as in Fig. 6 in the main part. Fig. 4c and Fig. 5a in the main part can be viewed as the top surface of the cube in (a) and (b), respectively (but for the fact that in Figs. 4c and 5a we have  $\alpha_1 = 1 = \alpha_2$  while at the top surface in (a) and (b) we obtain  $\alpha_1 = 0.925 = \alpha_2$ ). Together with Fig. 6, panels (a) and (b) are used to calculate the relative size of the parameter space resulting in the different evolutionary outcomes as reported in Table 1 in the main part. The following observations can be made. First, the position of the green surface in (a) is independent of  $z_h$  and  $z_\alpha$  while in (b) it is independent of  $z_\alpha$ . Thus, whether or not a singular point is invadable is independent of the trade-off curvature of the non-evolving traits, a fact that is also evident from Eqs. (B7) and (C6). Second the the boundaries indicating invadability and attractivity intersect with each other at the consumer extinction boundary. The reason is that at the extinction boundary the derivative of the equilibrium resource densities  $\hat{R}_i'(\theta_e^r)$  with the respect to the resident trait value  $\theta_e^r$  equal zero (see Eq. B5). This results in  $H = J$  at the corresponding trade-off curvatures (cf. B8 and C7). Other parameter values as in Fig. 6.